Assessment of different quantum mechanical methods for the prediction of structure and cohesive energy of molecular crystals

(Article begins on next page)

15 October 2023

Assessment of Different Quantum Mechanical Methods for the Prediction of Structure and Cohesive Energy of Molecular Crystals

Michele Cutini,[a] Bartolomeo Civalleri,[a,*] Marta Corno,[a] Roberto Orlando,[a] Jan Gerit Brandenburg[b], Lorenzo Maschio,[a] and Piero Ugliengo[a,*]

[a]*University of Turin, Department of Chemistry and NIS (Nanostructured Interfaces and Surfaces) Center, Via P. Giuria, 10125 Turin, Italy*

[b]*Mulliken Center of Theoretical Chemistry, Institut für Physikalische und Theoretische Chemie der Universität Bonn, Beringstraße 4, 53115 Bonn, Germany*

* e-mail: bartolomeo.civalleri@unito.it, piero.ugliengo@unito.it

Abstract

A comparative assessment of the accuracy of different quantum mechanical methods for evaluating the structure and the cohesive energy of molecular crystals is presented. In particular, we evaluate the performance of the semi-empirical HF-3c method in comparison with the B3LYP-D* and the Local MP2 (LMP2) methods by means of a fully periodic approach. Three benchmark sets have been investigated: X23, G60 and the new K7; for a total of 82 molecular crystals. The original HF-3c method performs well, but shows a tendency at overbinding molecular crystals, in particular for weakly bounded systems. For the X23 set, the mean absolute error for the cohesive energies computed with the HF-3c method is comparable to the LMP2 one. A refinement of the HF-3c has been attempted by tuning the dispersion term in the HF-3c energy. While the performance on cohesive energy prediction slightly worsens, optimized unit cell volumes are in excellent agreement with experiment. Overall, the B3LYP-D* method combined with a TZP basis set gives the best results. For cost-effective calculations on molecular crystals, we propose to compute cohesive energies at the B3LYP-D*/TZP level of theory on the dispersion-scaled HF-3c optimized geometries (i.e. B3LYP-D*/TZP//HF-3c(0.27) also dubbed as SP-B3LYP-D*). Beside, for further benchmarking on molecular crystals, we propose to combine the three test sets in a new one denoted as MC82.

Introduction

A molecular crystal may be seen as a periodic supramolecular entity for which all types of intermolecular interactions ranging from weak van der Waals forces to strong coordination bonds take place to interconnect molecules throughout space. The correct and balanced description of intermolecular forces is then crucial for the theoretical prediction of their structure and cohesive energy.[1–3] In particular, among intermolecular interactions, dispersion forces play a significant role in dictating the crystal packing and for crystal structure prediction.[4–8] Additionally, they are relevant in many chemical phenomena such as surface adsorption, supra-molecular chemistry and reactivity.[9–11] In last decades, it has become clear that an accurate description of dispersion interactions is necessary in order to perform reliable molecular simulations. Therefore, various methodologies that explicitly include dispersion forces have been presented during last years. Two recent review articles describe their different construction principles.[12,13]

In particular, this problem has plagued density functional theory (DFT) approximate methods, so that many dispersion-corrected schemes have been developed, such as the vdW-DFs, DFT-D, 1ePOT and, on a different level, double hybrid DFs (some of these methods are reviewed in Ref [9]). Among the dispersion-corrected methods, the most widely used are the DFT-D methods that employ a semi-classical treatment of dispersion energy. In particular, the D2 correction and its recent improved D3 scheme, both proposed by S. Grimme and coworkers, are the most widely applied. Some of these methodologies, first employed and tested on molecular benchmark sets, have then been transferred to the solid-state. Indeed the D2,[14] the D3,[8] the XDM[17], the MBD[18] and other methods are now available also for periodic calculations.

Recently, Sure and Grimme have proposed a robust semi-empirical method based on the Hartree-Fock (HF) method combined with a minimal basis set and three semi-empirical corrections, denoted as the HF-3c method. It has been demonstrated that HF-3c is capable to compute accurate interaction energies and geometries for molecular systems.[19] So far, the results published for molecular crystals did not include unit cell relaxation which is a crucial aspect for crystal structure prediction.[20,21]

A different, more robust yet computationally demanding approach to take into account dispersion forces is that of wavefunction (post-HF) methods. Despite the wide application of post-HF methods to molecular systems, their use for solids is still limited. Among post-HF methods, fully periodic MP2[22–24], random phase approximated and coupled cluster CCSD(T) correlation energies have been reported.[25–27] Nevertheless, only the periodic Local-MP2[22–24] (LMP2) implementation is today efficiently applicable in routine calculations. Interestingly, the LMP2 method[22] is also a component

of standard double hybrid density functionals and has been successfully applied for few systems.[28–31]

Molecular crystals represents an ideal benchmark to evaluate the accuracy of the theoretical prediction of intermolecular forces in solid-state. Computing cohesive energy and optimized cell volume of molecular crystals is nowadays affordable for medium-to-large molecular crystals and the comparison with experiment is facilitated because of the richness of available data. Recently, benchmark sets have indeed been proposed to assess the performance of ab initio methods for molecular crystals. For instance, a large body of recent literature exists on the X23 benchmark set, for which many computational tools have been tested.[15,32,33] This set includes 23 molecular crystals ranging from pure dispersion driven to mainly H-bonded systems. Beside the X23, other benchmark sets have been compiled like the G60 test set, that contains 60 molecular crystals including also computationally challenging systems such as halogenated and nitro compounds.

In this work, our goal is then to validate different computational methods for computing equilibrium cell volumes and cohesive energies of molecular crystals. In particular, we benchmark the accuracy of the low-cost empirical corrected HF-3c method and refine it for periodic systems by tuning its empirical parameters, as will be detailed in the next section. The hybrid DFT-D functional B3LYP-D* combined with a large basis set has been adopted as a theoretical reference method. Notably, the fully *ab initio* LMP2 method, employing a polarization augmented double zeta basis set, has been tested, in the present work, for the first time on the full X23 set. Furthermore, we propose a new methodology for computing fast and accurate molecular crystals properties, that can be applied for crystal structure prediction. As validation sets of molecular crystals we refer to the X23 set along with the extended G60 test set. In addition, we included a smaller set of seven molecular crystals, hereafter denoted as K7, which is proposed here for the first time.

Methodology

Brief review of the HF-3c method

In this section, we briefly recall the semi-empirical HF-3c method[19] investigated in the present study.

The HF-3c method consists in a Hartree-Fock calculation with the minimal quality basis set called MINIX and three semi-empirical corrections to the HF energy. The MINIX basis set includes different small sets of basis functions for different groups of atoms.[19] As a function of the chemical element, the valence scaled minimal basis set MINIS,[34] the split valence double-zeta basis set SV,

SVP,[35] and def2-SV(P)[36] are employed. The three correction terms are added in order to: (i) include long-range London dispersion interactions, (ii) correct for the basis set superposition error (BSSE) and (iii) correct for the short range basis set incompleteness (SRB). The first correction term, $E_{disp}^{D3(BJ)}$, is the semi-classical London dispersion energy from the D3 correction scheme[16] and applying the Becke-Johnson damping function (BJ),[17,37]

$$E_{disp}^{D3(BJ)} = -\frac{1}{2}\sum_{A \neq B}^{atoms}\left(s_6 \frac{C_6^{AB}}{R_{AB}^6 + (a_1 R_{AB}^0 + a_2)} + s_8 \frac{C_8^{AB}}{R_{AB}^8 + (a_1 R_{AB}^0 + a_2)}\right) \qquad (1)$$

where C_6^{AB} and C_8^{AB} are the dispersion coefficients for each atom pair AB at the 6th and 8th order, R_{AB} is their inter-nuclear distance and s_6 and s_8 are scaling factors. Moreover, the fitting parameter R_{AB}^0 is defined as $\sqrt{\frac{C_8^{AB}}{C_6^{AB}}}$, and the a_2 and a_1 terms are the cut-off radii.

The BSSE correction E_{BSSE}^{gCP} is evaluated in the geometrical counterpoise correction (gCP) scheme.[38] It consists in a semi-empirical, repulsive pair potential which decays exponentially with the interatomic distance R_{AB}

$$E_{BSSE}^{gCP} = \sigma \sum_{A}^{atoms} \sum_{A \neq B}^{atoms} e_A^{miss} \frac{exp\left(-\alpha(R_{AB})^\beta\right)}{\sqrt{S_{AB} N_B^{virt}}}$$

e_A^{miss} measures the incompleteness of the atomic target basis set. The potential is normalized by the Slater-type overlap S_{AB}, the number of virtual orbitals N_B^{virt}, and the empirical parameters α and β. The sum over all atoms is then weighted by a global scaling parameter σ.

The E_{SRB} is included for rectifying the covalent bond length that is systematically overestimated for electronegative elements when HF with MINIX basis set is used, due to the small size of the basis set.

The corrected total energy, HF-3c, is then calculated as

$$E_{tot}^{HF-3c} = E_{tot}^{HF/MINIX} + E_{disp}^{D3(BJ)} + E_{BSSE}^{gCP} + E_{SRB} \qquad (2)$$

Despite its semi-empirical character, the method presents several advantages: (i) it is very fast due to minimal basis, (ii) it provides on average correct bond length, (iii) it is self-interaction error free and (iv) it is purely analytical (grid free) thus leading to noise free derivatives. However, no Coulomb correlation is included thus leading to limited applicability for electronically complicated systems and the too small basis set could be not enough to describe anionic systems.

Nevertheless, we pursued to improve the performance of the HF-3c method by scaling the $E_{disp}^{D3(BJ)}$ and the E_{BSSE}^{gCP} contributions in eq. 2. In the first case, the s_6 term was kept fixed to unity to enforce

the correct asymptotic limit of the leading term in the $-\frac{1}{R_{AB}^6} - \frac{1}{R_{AB}^8} ...$ dispersion energy series, whereas the s_8 term was reduced by a factor of 0.7, 0.5 and 0.27 (see eq. 1). In the second case, an overall scaling term σ of 1.23 was applied. Experimental values for graphite exfoliation energy and interlayer distance were used as reference values to scale the s_8 factor in the dispersion term, while the gCP scaling factor was obtained through a best fit of the counterpoise corrected curve. Further details of the fitting procedure are reported in the supporting information. No attempts were pursued to modify the short-range term that is not expected to influence intermolecular interactions. Geometry optimizations were re-run for both the molecules and the crystals with scaled parameters.

Computational details

All HF-3c calculations were performed with a development version of the CRYSTAL14 code.[19,39] For comparison, we also run calculations with the dispersion corrected B3LYP-D* hybrid functional[40–42] by using the TZP basis set devised by Ahlrichs and co-workers.[35] As a further validation, we also tested the B3LYP functional in combination with the D3 correction both without and with the Axilrod–Teller–Muto (ATM)-three-body-term[43,44] (D3[ABC]).[16]

In addition, we performed wavefunction based *ab initio* calculations employing the second order Møller-Plesset perturbation theory (MP2)[45] as implemented in the CRYSCOR code.[22] Here, a development version of the code has been used which employs Orbital-Specific Virtuals (OSV)[46,47] for the definition of the virtual space. A 6-31G basis set plus polarization functions and augmented with diffuse polarization functions (hereafter denoted as p-aug-6-31G(d,p)) has been adopted. See SI for further details.

The visualization of structures was done with MOLDRAW version 2.0.[48] Images were produced with VMD version 1.9.2.beta1.[49]

Computational parameters for geometry optimization and vibrational frequency calculation

An unconstrained relaxation of both atomic coordinates and cell parameters was performed for all considered set of molecular crystals by keeping the symmetry of the system. Atomic positions and cell vectors were optimized using the analytical gradient method. The Hessian was upgraded with the Broyden-Fletcher-Goldfarb-Shanno (BFGS) algorithm.[50–52] Tolerances for the maximum allowed gradient and the maximum atomic displacement for convergence were kept at the default

values (0.00045 Ha·bohr^{-1} and 0.00030 Bohr, respectively). For the vibrational frequency calculations, the mass-weighted force-constant matrix was computed at the Γ point by numerical derivative of the analytic nuclear gradients. A value of 0.003 Å was chosen as the displacement of each atomic coordinate and the tolerance for the SCF cycle convergence was tightened from 10^{-7} to 10^{-11} Ha. Values of the tolerances that control the Coulomb and exchange series in periodic systems[53] are reported in Table S1 and S2 of the SI. The Γ-centered k-point grid is generated via the Monkhorst−Pack scheme[54] with a system dependent number of k points. More details on the number of k points used in the calculations are reported in Table S1 of the SI. The eigenvalue level-shifting technique was used to lock the system in a non-conducting state,[53] with level shifter set to 0.6 Ha. To help convergence of the SCF, the Fock/KS matrix at a cycle was mixed with 30% of the one of the previous cycle.[53] The thresholds ITCOUL and ITEXCH, governing the bipolar approximation, were set to 18/14 and 14/10 for the B3LYP/HF-3c simulation, respectively.[53] The electron density and its gradient were integrated over a pruned grid consisting of 974 angular and 75 radial points generated through the Gauss–Legendre quadrature and Lebedev schemes.[55]

Cohesive energy and sublimation enthalpy

Since the calculation of the cohesive energy, ΔE_c, is one of the main target of this work, we briefly detail how we compute it and compare it to the experimental sublimation enthalpy.

The cohesive energy is defined as:

$$\Delta E_c = E_{cry}/Z - E_{mol} \quad (3)$$

where E_{cry} is the total energy of the crystal unit cell with optimized cell parameters and internal coordinates, Z the number of molecules in the unit cell, and E_{mol} is the total energy of the fully optimized isolated molecule in the gas phase.

The DFT and LMP2 computed cohesive energies were corrected for the BSSE by the counterpoise method (CPC).[56] As shown above, the HF-3c method is inherently BSSE corrected, therefore no further correction was included.

Computed cohesive energies were compared with thermodynamically back-corrected experimental sublimation enthalpies. For the X23 set, the back-correction procedure took into account the thermal and zero point vibrational energy explicitly by following Reilly and Tkatchenko's work.[33] For the G60 and K7 sets, the experimental cohesive energies were estimated by subtracting a constant factor 2RT to the experimental sublimation enthalpy:

$$\Delta E_{exp} = \Delta H_{exp} - 2RT \quad (4)$$

or 3/2RT for linear molecules.

As a further check of the HF-3c method for the X23 set, instead of comparing computed results with thermodynamically back-corrected experimental sublimation enthalpies, we directly estimated the sublimation enthalpy and compared it to the experimental values.[57] To compute it, we used the following expression:

$$\Delta H_{sub} = -\Delta E_c + \Delta E_{vib} + 4RT \qquad (5)$$

where the constant term is 7/2 RT for linear molecules and ΔE_{vib} includes both the zero point energy (ZPE) and the thermal vibrational energy contributions. This expression is true only when the isolated molecule has a well-defined conformation at a given temperature, behaves as an ideal gas and no phase transformation occurs between 0 K and T. We calculated the vibrational frequencies in the harmonic approximation for the molecule in the crystal and in the gas-phase. To compute the thermal vibrational contribution to enthalpy for molecular crystals the Einstein model has been applied. In this model, each phonon branch is approximated with a single frequency obtained at the Γ point, the acoustic ZPE is neglected and the acoustic thermal energy is evaluated at the high temperature limit as 3RT.[32]

Results and discussion

In the following, we report and discuss the computed properties (i.e. unit cell volume, cohesive energy and sublimation enthalpy) for the molecular crystals in three benchmark sets investigated in the present work, namely: the X23, the G60 and the K7 sets (see Table S4 for details about crystal structures and corresponding experimental data).

For the following discussion, it is crucial to keep in mind the uncertainties in the reference values. Measured sublimation enthalpies are typically accurate within 4.2 kJ/mol[58] and a comparison of the '2RT correction' with explicitly calculated zero-point vibrational and thermal contributions adds up (assuming uncorrelated error sources) to a total uncertainty of about 4.5 kJ/mol. While anharmonic effects can in principle lead to an additional systematic error, we expect its overall effect to be minor. In contrast, the measured unit cell volumes at finite temperatures (between 10 and 298 K) are systematically shifted. As the intermolecular potentials of organic molecules typically exhibit a slight asymmetry with smaller curvature at longer distances, most organic crystals expand under heating. For small molecules the intermolecular distances have a most pronounced contribution to the crystal unit cell and the corresponding thermal expansion of those coordinates translates in substantially larger unit cell volumes. In contrast, for larger molecules the molecular size has a significant contribution and the corresponding covalent potentials exhibit a smaller thermal expansion. The thermal expansion from zero-point exclusive 0K to room temperature has been

estimated for various systems to range between 1 and 8%.[59–62] It is important to note that we compare the geometries calculated on the purely electronic energy surface with the measured ones corresponding to a free energy surface. Given the above discussed systematic shifts, too small unit cell values are actually 'correct'. However, since we know that several studies conduct this direct comparison,[63–65] we want to present a pragmatic strategy to implicitly account for these effects. In this regard, the re-parametrization of HF-3c is similar to the B3LYP-D* strategy, where the dispersion part is empirically scaled to reproduce experimental geometries. In addition to the zero-point vibrational and thermal effects, certain many-body London dispersion effects are absorbed into an effectively reduced two-body dispersion.

Hereafter, we will discuss the unit cell volume in relative percentage unit, whereas cohesive energies and sublimation enthalpies are discussed in energy unit. We do this to avoid the effect on the statistics of some molecular crystals belonging to the G60 benchmark set with very large experimental unit cell. The details of the statistical functions are reported in the SI.

X23 set

The X23 set includes 23 molecular crystals. The data set originates from the C21 benchmark set compiled by Otero-de-la-Roza and Johnson[32] that was, later, extended with two additional molecular crystals (i.e. succinic acid and hexamine) by Reilly and Tkatchenko.[33] Table S5 in the Supporting Information reports the list of molecular crystals included in the X23 set. In the analysis of the molecular crystal structures of the X23 set, we realized that the rhombohedral polymorph of triazine (phase I) included in the X23 and C21 sets, is not stable at low temperature. It undergoes a phase transition at about 200K to a monoclinic polymorph, the so-called phase II. B3LYP-D* and HF-3c calculations on the triazine polymorphs support the experimental evidence. Indeed, the phase II is 1.1 and 2.3 kJ·mol^{-1} more stable than the phase I at the B3LYP-D*/TZP and HF-3c-(0.7 s_8) level, respectively. When the zero point energy is included at the HF-3c-(0.7 s_8) level, the phase II results to be more stable by 1.5 kJ·mol^{-1}. Therefore, in the following comparison between computed and experimental data, we employ triazine phase II in the analysis of cell volumes. Instead, for consistency with previous benchmarking works on the X23 set, we refer to triazine phase I when comparing cohesive energies and sublimation enthalpies.

Let us first compare the results for the HF-3c and the B3LYP-D*/TZP methods. In both cases, we refer to the fully optimized crystal geometry. Table 1 reports the statistical summary of the predicted cell volumes compared with the available experimental data. To better appreciate the role of the different intermolecular interactions, the X23 set of structures has been divided into three

groups according to the predominant type of contributions to the binding energy, namely: dispersive interactions, hydrogen-bonding interactions and mixed interactions.

In Figure 1, we illustrate the relative deviations in percentage of the HF-3c and B3LYP-D*/TZP optimized crystal cell volumes from low temperature experimental data. As expected, HF-3c shows a systematic tendency to shrink the unit cell volume with respect to experiment. This contraction effect is larger for the systems in which dispersion forces are more important, e.g. dispersion dominated subgroup (crystal label 1-10) and mix subgroup (crystal label 20-23). Those systems are indeed the main source of error in the statistics for the HF-3c method (see Table 1). The strongest differences can either arise due to an intrinsic error of HF-3c or due to the typically more shallow potential of pure π-systems in contrast to hydrogen bonded ones. In contrast, but not unexpectedly, the B3LYP-D*/TZP method performs better. The computed mean absolute relative error in percentage (MARE%) is 3.0% and the distribution around the mean value is narrower than HF-3c with a percentage standard deviation (SD%) of 1.9%.

The statistic of the cohesive energies of the X23 set calculated with HF-3c and B3LYP-D*/TZP is shown is Table 2. Figure 2 shows the deviations of the computed from the measured cohesive energies. Even though the cohesive energies for the X23 set have been previously reported for the HF-3c method,[20,66] the corresponding values, ΔE_c, for the fully optimized geometries have never been presented before. As an additional comparison, we report the same analysis as obtained by other authors with the PBE0-MBD (on the optimum PBE+TS geometry) and PBE-D3 methods with complete basis set of projector augmented plane-waves, and PBE-D3 and B3LYP-D3 methods with a SVP basis set and the empirical gCP scheme to correct the cohesive energies for the BSSE.[33,67]

The accuracy of HF-3c in computing the cohesive energy for the whole X23 set as given by a mean absolute error (MAE) of 8.2 kJ·mol^{-1} is comparable with DFT methods with small basis sets B3LYP-D3-gCP/SVP and PBE-D3-gCP/SVP that, show a MAE of 7.8 and 10 kJ·mol^{-1}, respectively. As observed for the unit cell volumes, HF-3c gives the largest deviation for systems dominated by dispersion interactions (MAE 10.3 kJ·mol^{-1}). In that case, indeed, computed ΔE_c are clearly overestimated as shown by a mean signed error of 9.4 kJ·mol^{-1}.

Remarkably, the B3LYP-D*/TZP method performs very well. We attained a MAE of 4.6 kJ·mol^{-1} for the X23 set that is close to the "chemical accuracy" (i.e. 4.2 kJ·mol^{-1}).[58] Other dispersive corrected DFT methods that employ large basis sets of plane-waves such as PBE0-MBD/CBS and PBE-D3/CBS reach similar accuracies.

Despite the reasonably good performance of the HF-3c method, results show that there is room for even further improvement. As previously pointed out, on one hand, HF-3c tends to predict unit cell

volumes that are systematically smaller than experiment, on the other hand, computed cohesive energies are overestimated. The HF-3c method has been parametrized on molecular adducts which differ from the systems studied in this work. In molecular crystals the overlap between charge densities is larger and the intermolecular contacts are shorter. This may lead to an unbalance combination of the semi-empirical terms that are expected to have larger effects on modeling intermolecular interactions for the dispersion and the gCP corrections. Additionally, we want to develop a practical strategy to directly compute X-ray geometries (compare with discussion on thermal expansion given above). Therefore, we attempted to scale both terms of the HF-3c method. We first enforced the correct asymptotic limit by fixing the s_6 factor to one, whereas the s_8 term was reduced by a factor of 0.7, 0.5 and 0.27 (see eq. 1). The resulting methods have been denoted as HF-3c-(0.7 s_8), HF-3c-(0.5 s_8) and HF-3c-(0.27 s_8). Secondly, an overall scaling term σ of 1.23 was applied to the gCP term and referred to HF-3c-(1.23 gCP).

Geometry optimizations were re-run for both the molecules and the crystals with the modified HF-3c methods with scaled parameters. The corresponding statistical analysis is gathered in Table 1. The volumes computed with the scaled dispersion term are in better agreement with the experiment than the pure HF-3c. As expected, the scaling of the s_8 factor leads to a systematic expansion of the cell volume due to the reduced binding energy within the crystal. The MARE% of 8.0% for HF-3c, now, drops to 1.9% for HF-3c-(0.27 s_8). It is worth noticing that the percentage standard deviation does not change when tuning the dispersion term. The scaling procedure leads to a progressive reduction of the mean relative error in percentage (MRE%) (i.e. -8.0%, -5.2%, -3.2% and -0.8% for the HF-3c, HF-3c-(0.7 s_8), HF-3c-(0.5 s_8) and HF-3c-(0.27 s_8) methods, respectively) and this is the reason of the increased accuracy. Notably, the HF-3c-(0.27 s_8) computes molecular crystal volumes closer to experiment than the B3LYP-D*/TZP method. An expansion of the computed volumes is also obtained when increasing the BSSE correction in the HF-3c method through the gCP term. It turnout that the HF-3c-(1.23 gCP) predicts unit cell volumes with good accuracy thus reaching a MARE% of 5.6%.

As the volume analysis suggests, when decreasing the dispersive contribution to the HF-3c total energy leads to cohesive energies in closer agreement with the experiment. The HF-3c-(0.7 s_8) method reduces the MAE from 10.3 to 4.5 kJ·mol^{-1}, for the dispersion dominated systems. This scaling increases the overall accuracy thus yielding a MAE of 6.9 kJ·mol^{-1}. These results and those for the optimized unit cell volumes may point out the need of new fitting parameters specific for solid state systems. It is clear that semi-empirical methods cannot be parametrized to yield generally good results for all possible observables, so we aim here at a specialized version with improved crystal mass densities (related to the intermolecular distances) and cohesive energies.

A further reduction of the dispersion term, i.e. 0.5 and 0.27 scaling factors, leads to a loss of binding energy within the crystals, with a general underestimation of the ΔE_c. The computed MAE are 8.8 and 13.1 kJ·mol^{-1} for HF-3c-(0.5 s_8) and HF-3c-(0.27 s_8), respectively. The HF-3c-(1.23 gCP) method shows a better balanced accuracy in computing the ΔE_c for the different X23 subsets, but it is in general less accurate than the original HF-3c. The best performance, on average, is achieved by scaling the s_8 term by a factor of 0.7. This leads to the best results for crystal structures and the best evaluation of the cohesive energy with respect to all HF-3c methods. Therefore, from now on we refer to the scaled version as S-HF-3c method.

In addition, since the HF-3c-(0.27 s_8) resulted to give the best crystal structures among the HF-3c scaled variants, the cohesive energies for the X23 were also computed through single-point energy calculations at the B3LYP-D*/TZP level on the HF-3c-(0.27 s_8) optimized structures. This approach has been denoted hereafter as SP-B3LYP-D*. Encouraging, high accuracy is achieved by this approach, which shows a MAE of 5.2 kJ·mol^{-1} with a SD of 5.8 kJ·mol^{-1}. Similarly, we also tried on the S-HF-3c optimized geometries. In this case, results are slightly worsened with a MAE of 5.5 kJ·mol^{-1} with a SD of 6.2 kJ·mol^{-1}. Overall, the combination of single-point energy calculations at the B3LYP-D*/TZP level on the HF-3c geometries is a very promising result. Indeed, this paves the way to its application in crystal structure prediction due to the very cheap cost of crystals geometry optimization, in particular at the HF-3c-(0.27 s_8) level.

As another important benchmark in the present work, we computed the cohesive energies of the X23 set at the LMP2 level of theory, for the first time. In this case, single-point energy calculations were carried out on the B3LYP-D*/TZP optimized structures by using a p-aug-6-31G(d,p) basis set (LMP2/p-aug-6-31G(d,p)). Since the LMP2 energy includes electron correlation effects, we expected that the LMP2 method would give a proper description of intermolecular dispersion forces. The LMP2/p-aug-6-31G(d,p) method performs moderately well in computing the cohesive energies. However, the accuracy is lower than most of the methods presented above with a MAE of 9 kJ·mol^{-1} and a SD of 11 kJ·mol^{-1}. Even though, LMP2 performs best in the description of systems with mixed-type interactions (see Table 2). Again, two effects may lead to these deviations. On the one hand, the basis set may be too small and far from complete for a correlated wavefunction method, which is however needed to make to computations feasible. On the other hand, MP2 intrinsically performs badly for dispersion dominated interactions, in particular for chemically unsaturated systems.[68,69] The reason for this is that the dispersion energy contribution to the supermolecular MP2 energy lacks intramolecular correlation effects and therefore describes the long-range correlation energy on the so-called uncoupled level.

To better understand the basis set dependency of LMP2 , we further investigated the systems with very high percentage error (over 20%), namely CO_2 and pyrazine. As regards CO_2, the cohesive energy is underestimated by 20.2%, but it is know that the result can be improved by enlarging the basis set size,[29] whereas, for pyrazine, the cohesive energy is overestimated by 43.0%. The interaction energy of a dimer extracted from the B3LYP-D*/TZP optimized crystal was performed at the LMP2 level by employing the p-aug-6-31G* and the larger aug-cc-pVTZ (without diffuse s functions). The dimer binding energy decreases from 16 kJ·mol^{-1} to 12 kJ·mol^{-1} by increasing the basis set size. If the same correction were applied to the cohesive energy of the crystal the percentage error would reduce to 7%. Thus, even in the converged basis set, we expect an overestimation of cohesive energies for π-systems as explained above. Apparently, one has to go beyond MP2 to achieve an accuracy that is consistently higher compared to dispersion corrected density functionals.

As picture of the overall accuracy of the investigated methods, the plot of the normal error distributions has been illustrated in Figure 3. It highlights that the full width at half maximum of the HF and Post-HF methods is similar. While the LMP2 method tends to underbind, the HF-3c method tends to overbind the molecular crystals. For the HF-3c method, as discussed above, an unbalanced contribution to intermolecular energy (i.e. dispersion and gCP) in solid state calculations could explain the systematic overestimation of ΔE_c. In fact, by simply tuning the s_8 term, like for the S-HF-3c method, the normal error distribution becomes narrower and more centered around the zero value. As regards DFT methods, the B3LYP-D*/TZP and the SP-B3LYP-D* approaches present very sharp and centered distributions of errors, comparable to the PBE-D3/CBS method. This is not unexpected because for all DFT calculations a dispersion correction was included and large basis sets were employed.

To further analyze the accuracy of the HF-3c method in computing the properties of molecular crystals we have evaluated the sublimation enthalpies, ΔH_{sub}, for the X23 set. For the HF-3c and S-HF-3c methods computed cohesive energies were corrected by including the thermal contribution to enthalpy (ΔE_{vib} + 4RT). In Figure 4, we compare the results obtained for the S-HF-3c with the PBE+TS results and the widely adopted 2RT correction.[70] We also considered a reduced ΔE_{vib} contribution by scaling the zero point and thermal energy to account for the systematic error of the HF method in computing the vibrational frequencies. By following the work of Sinha et al.[71] a factor of 0.9204 and 1.1254 were adopted for zero-point and thermal energies, respectively. Figure 4 shows that the S-HF-3c computed thermal corrections for the different molecular crystals are in good agreement with the PBE+TS results. Interestingly, the best agreement is reached for the

dispersive subgroup. It is important to point out that, on average, the thermal correction to enthalpy is -7.1 kJ·mol^{-1} and -6.3 kJ·mol^{-1} for S-HF-3c and PBE+TS, respectively. These values are not far from the 2RT constant correction (about -5.0 kJ·mol^{-1}). This then suggests that such correction can be used as an easy and fast way to estimate experimental cohesive energies from the experimental sublimation enthalpies without the need of expensive vibrational frequencies calculations. In that case, one can assume an error bar of 2.0 kJ·mol^{-1}. The statistical analysis for the ΔH_{sub} is summarized in Table 3. It can be seen the HF-3c method yields sublimation enthalpies with reasonable accuracy with a MAE of 8.6. In addition, our proposed scaling method, S-HF-3c, further improves the accuracy by achieving a MAE of 7.3 kJ·mol^{-1}. Results in Table 3 and Figure 4 also show that the scaling of the vibrational quantities does not lead to any change in our results.

G60 set

The G60 set is an extended benchmark set of 60 molecular crystals employed for the first time by Gavezzotti and some of us, few years ago,[70] which includes molecules with a wide range of chemical functionalities. Thus it represents a challenging validation test for computing non-covalent interactions. The analyzed systems are listed in Table S4 of the SI. We notice that 8 out of the G60 systems belong also to the X23 set.

We investigated the performance of the HF-3c, S-HF-3c and HF-3c-(0.27 s_8) methods in computing the cohesive energy and the unit cell volumes of all the 60 molecular crystal in the benchmark set. The statistical analysis of the predicted unit cell volumes is reported in Table 4. Details are given in Table S6 of the SI. The results we obtain for the G60 set parallel those obtained for the X23 set. It is confirmed that when tuning the dispersion term within the HF-3c approach the accuracy improves, without any relevant change in the SD% of the method. In fact, for the G60 set, we compute MARE% of 6.9%, 4.7% and 3.5% at the HF-3c, S-HF-3c and HF-3c-(0.27 s_8) levels, respectively, to be compared with the values of 8.0, 5.2% and 1.9% for the X23 set. Instead, the MRE% are shifted to higher values compared to those for the X23 set. We calculate a MRE% of -6.7%, -3.8% and +0.7% for the G60 set and of -8.0%, -5.2% and -0.8% for the X23 set at the HF-3c, S-HF-3c and HF-3c-(0.27 s_8) levels, respectively. A closer inspection of the results shows that this positive shift may be due to chlorinated compounds whose interaction energies appear to be not properly reproduced by the methods investigated in the present work. The HF-3c-(0.27 s_8) method, which does very well in computing unit cell volumes for the X23 set, gives indeed volumes of the chlorinated molecular crystals that are 3% larger, on average, than experiment. This overestimation is also observed for nitro-substituted compounds. In both cases, we believe that this is due to the electron rich moieties whose complex chemical behavior (e.g halogen-halogen interactions) needs

both the inclusion of correlation effects missing in HF-3c and larger basis sets to be properly described.

Along with HF-3c and S-HF-3c, we computed the cohesive energy with the SP-B3LYP-D* approach. The statistical analysis is reported in Table 5. Details can be found in Table S7 of the SI. As a comparison, we have also included the results for the ΔE_c at the B3LYP-D*/6-31G* method calculated by keeping the crystal and molecules geometries fixed to the experiments, as reported in ref [70]. In this case, the scaling of the dispersion term in the HF-3c scheme does not lead to any improvement. In fact, the computed MAE is 12 kJ·mol^{-1} for both the standard and scaled methods. The performance of the B3LYP-D* method improves when increasing the basis set size. This is testified by the MAE of 8.8 kJ·mol^{-1} and 10 kJ·mol^{-1} at the SP-B3LYP-D*, which employs a TZP basis set, and B3LYP-D*/6-31G* levels, respectively. It must be noticed that the accuracy achieved in computing the G60 set cohesive energies is rather poor in comparison to the results obtained for the X23 set. For instance, the computed S-HF-3c MAE is 12 kJ·mol^{-1} for G60 benchmark set while it is 6.9 kJ·mol^{-1} for the X23 set. We suspect that G60 cohesive energies are predicted with low accuracy and precision for mainly two reasons. Firstly, the experimental error on the sublimation enthalpies used as reference data for the statistical analysis, is larger than for the X23 dataset. Secondly the nitro and chlorinated compounds, which have shown large deviations from experiment for the crystal structure, cannot be properly simulated with both the original and scaled HF-3c methods assessed in this work.

K7 set

The K7 set is comprised of seven molecular crystals selected because of the different intermolecular interactions present in the structure, namely: acetamide, the cubic and orthorhombic polymorphs of acetylene, boric acid, hydrogen cyanide, ice XI and propane. We optimized crystal structures at the HF-3c, S-HF-3c, HF-3c-(0.27 s_8) and B3LYP-D*/TZP levels and then computed the corresponding cohesive energies. For the HF-3c-(0.27 s_8) method the SP-B3LYP-D* approach was adopted. For brevity, the results and the statistical analysis are gathered in Table S8 in the supporting information.

As already seen for the X23 and the G60 sets, the HF-3c method tends to overestimate dispersion interactions so that it systematically underestimates the unit cell volumes. Instead, the HF-3c-(0.27 s_8) method predicts unit cell volumes in good agreement with the B3LYP-D*/TZP method. In fact,

the latter performs slightly better than the HF-3c-(0.27 s_8) with the computed MARE% being 3.2% and 5.3%, respectively.

The trend for the computed cohesive energies of the K7 set parallels the one of the other test sets. As already pointed out, when decreasing the dispersion within the HF-3c approach the accuracy increases. For instance, the MAE for the HF-3c method of 8.1 kJ·mol^{-1} decreases to 6.2 kJ·mol^{-1} for S-HF-3c, although, both the unscaled and scaled HF-3c methods are not as accurate as the B3LYP-related methods which give a MAE of 4.1 kJ·mol^{-1} and 4.0 kJ·mol^{-1} at the SP-B3LYP-D*/TZP and the B3LYP-D*/TZP levels, respectively. Notably, the proposed combination of scaled HF-3c geometries and B3LYP-D*/TZP energies as in the SP-B3LYP-D*/TZP approach confirms to give remarkably accurate cohesive energies also for the K7 set.

Molecular crystals geometry

Computed results highlight, clearly, the overall ability of the scaled HF-3c methods in predicting unit cell volumes. As a further assessment, we analyzed the intermolecular distances for a small selection of molecular crystals for which accurate experimental data are available from low-temperature neutron diffraction measurements,[72–75] namely: urea, formamide, fomic acid and benzene. They are also representative of different intermolecular interactions that lead to a different crystal packing from a 3D network of H-bonds in urea to 2D sheets of H-bonded molecules connected through weak CH---O bonds in formamide, from 1D H-bonded chains of formic acid linked by weak interchain interactions to a purely dispersive crystal as benzene. The most relevant intermolecular distances data have been gathered in Table 6 and shown in Figure 5. For the scaled HF-3c approach, the decrease of the dispersion contribution leads to an elongation of the intermolecular distances that are in a better agreement with the experimental values than the original HF-3c method. Overall, the B3LYP-D*/TZP predicts molecular crystal geometries in rather good agreement with experiment. Notably, the results for the HF-3c-(0.27 s8) method nicely approach those obtained at the B3LYP-D*/TZP level. This is a further demonstration of the validity of the SP-B3LYP-D* approach that relies on the HF-3c-(0.27 s_8) computed geometries.

Different dispersion schemes as applied to B3LYP-D

As a final assessment, we have explored the inclusion of the more recently proposed D3 correction without and with the Axilrod-Teller-Muto three-body term (hereafter denoted as D3^{ABC}) to the

B3LYP/TZP cohesive energies as computed on the scaled HF-3c-(0.27 s_8) optimized geometries for both the X23 and the G60 sets. The statistics are reported in the supporting information (see Table S9). While B3LYP-D3 performs worsen than B3LYP-D*, in the B3LYP-D3^{ABC}/TZP//HF-3c-(0.27 s_8) approach the inclusion of the repulsive three-body term reduces the over-binding tendency of the D3 scheme and leads to a MAE which is the lowest among the tested methods. For the X23 set, a remarkably low MAE of 3.5 kJ·mol^{-1} has been attained which competes with results found in literature, as for instance the PBE0/MBD method.[33] This intriguing result deserves further investigation and will be explored in a forthcoming work. One very strong advantage of the B3LYP-D/TZ approach when compared to commonly used GGA functionals as PBE-D/TZ (or PBE-MBD) is the inclusion of HF exchange that leads to (i) improved description of induction effects important to describe strong hydrogen bonds for e.g. water and ice and (ii) improved reaction barriers and thermochemistry needed to describe chemical reactions in the solid state. As alternative to using B3LYP-D/TZP, the recently proposed PBEh-3c method, a hybrid functional which employs a DZ quality basis set that includes the D3 and the gCP correction as HF-3c, could be another possible choice in the trade-off between cost and accuracy.[59]

Conclusions

In this work, we have presented a comprehensive evaluation of the performance of the semi-empirical HF-3c method and the dispersion-corrected B3LYP functional for the prediction of structure and cohesive energy of molecular crystals. Three benchmark sets, all envisaging molecular crystals, have been investigated: X23, G60 and the new K7; that is 82 molecular crystals in total. For comparison, the LMP2 post-HF method has been also investigated to assess its performance in reproducing the cohesive energies of the molecular crystals in the X23 set.

In summary, the following conclusions can be drawn.

Despite its simplicity, the semi-empirical HF-3c method gives accurate geometries and cohesive energy. We have found out a systematic tendency to overbind molecular crystals in which dispersion interaction tends to dominate. As a practical strategy, a simple scaling of the dispersion term, in particular for the -C_8/R^8 contribution, has been proposed that significantly improves the results. The best compromise for structure and cohesive energy has been obtained when applying a scaling factor of s_8=0.7 (S-HF-3c). The dispersion corrected B3LYP-D* functional confirms its excellent accuracy in predicting both structure and cohesive energy of molecular crystals, in

16

particular, when large basis sets are employed (e.g. TZP), even though the cost can rapidly increase with the size of the system. This latter point can be mitigated by adopting the very fast HF-3c-(0.27 s_8) method for structure prediction coupled with single point energy evaluation at the B3LYP-D* to predict cohesive energy (SP- B3LYP-D*). The saving in computational time is very large as for the most complex pyrazine crystal the HF-3c method is 36 times faster for a complete self-consistent field and nuclear gradient calculation with respect to B3LYP-D*/TZP. The computational burden increases in the following order HF-3c > B3LYP-D/TZ = PBE-D/CBS > MP2/TZ. Therefore, the SP-B3LYP-D* method proposed by us can be suggested as a cost-effective tool for studying molecular crystals.

For the X23 set, the LMP2 gives cohesive energies with only a moderate accuracy (but quite good for systems with mixed-type interactions). The non-excellent performance could be partly due to the small basis set employed (i.e. p-aug-6-31G(d,p)), that was chosen to keep the computational cost relatively low, and partially due to the intrinsic flaw of MP2 to describe dispersion interactions with the uncoupled HF orbitals and at the same time neglecting type-B non-additivity effects.[76] Nevertheless, promising results for molecular crystals were recently obtained with double hybrid methods[28,31] that are strictly related to MP2. Some of us showed indeed that different variants of double hybrids could outperform MP2.[28] Work is in progress to benchmark double hybrid functionals for the X23 set.

We also tested different DFT-D type corrections to B3LYP/TZP method. The B3LYP-D3[ABC]/TZP//HF-3c-(0.27 s_8) approach has been shown to be quite promising and deserves further investigations.

By combining the three test sets, we propose a new large benchmark set of molecular crystals, dubbed MC82. The reference cohesive energies have been estimated from the experimental sublimation energies by applying the 2RT correction factor. We have shown for the X23 set that, on average, such correction is not far from the thermal contribution to enthalpy obtained through rather costly vibrational frequencies calculations. Therefore, we have confidently applied this correction to other systems in the MC82 test set. Performance of the HF-3c method has been confirmed for the full set (see Table S10 in the supporting information), as well as the excellent agreement with experiment for the optimized unit cell volumes computed with the scaled HF-3c-(0.27 s_8) method. Overall, the SP-B3LYP-D* approach gives a good accuracy with a global MAE of 7.4 kJ/mol. Interestingly, as shown by preliminary results, the inclusion of the D3[ABC] correction to B3LYP/TZP would presumably provide quite accurate results.

In perspective, the combination of the cost-effective HF-3c method and the more accurate dispersion-corrected B3LYP/TZP model is potentially of great interest for large screening studies, in investigating polymorphism in molecular crystals[77] and in crystal structure prediction.

Acknowledgements

Supporting Information

Supporting information includes details on MP2 calculations, statistical functions, computational parameters for HF-3c and B3LYP calculations (Tables S1 and S2) and HF-3c scaling factors (Table S3). The list of molecular crystals is reported in Table S4. Full computed data and deviations from reference data for the X23, G60 and K7 sets are gathered in Table S5, S6, S7 and S8. Results of the comparison of different dispersion schemes for X23 and G60 sets are reported in Table S9. Summary of statistical analysis for volume and cohesive energies of the full MC82 set of molecular crystals (Table S10). This information is available free of charge via the Internet at http://pubs.acs.org/.

Table 1. Statistical summary for unit cell volumes of the molecular crystals in the X23 set. MAE, corrected sample standard deviation (SD) and maximum error (MAX) of the optimized volumes evaluated at the HF-3c and the B3LYP-D*/TZP levels of theory. For the HF-3c case, the results obtained by different scaling of dispersion and gCP terms are also reported (see text for details). The statistics is reported for both absolute errors (in Å^3) and relative absolute percentage errors by using the following format MAE ± SD (MAX). Details on the statistical functions employed in the SI.

	All (X23)	Dispersive	H-bond	Mixed
Statistics in Å^3				
HF-3c	27 ± 14 (-51)	33 ± 12 (-50)	15.2 ± 6.5 (-29.)	40.4 ± 7.6 (-50.6)
HF-3c-(0.7 s_8)	17.3 ± 9.4 (-34.3)	22.2 ± 8.6 (-34.3)	8.6 ± 3.7 (-15.4)	24.8 ± 2.7 (-28.7)
HF-3c-(0.5 s_8)	10.4 ± 7.2 (-23.1)	14.8 ± 6.6 (-23.1)	4.1 ± 2.7 (-9.3)	13.8 ± 5.6 (-19.4)
HF-3c-(0.27 s_8)	5.9 ± 6.7 (16.2)	7.2 ± 5.2 (-10.6)	3.4 ± 3.7 (-6.3)	9 ± 11 (16)
HF-3c-(1.23 gCP)	19 ± 13 (-44)	26 ± 11 (-44)	7.8 ± 5.8 (-20.6)	30.2 ± 5.1 (-36.1)
B3LYP-D*/TZP	10.1 ± 8.7 (-35.7)	12.6 ± 9.8 (-35.7)	5.4 ± 4.6 (-14.5)	14.6 ± 9.7 (-22.3)
Statistics in percentage				
HF-3c	8.0 ± 2.5 (-12.4)	9.2 ± 2.5 (-12.4)	6.5 ± 2.3 (-12.2)	8.3 ± 1.2 (-9.7)
HF-3c-(0.7 s_8)	5.2 ± 2.3 (-9.5)	6.4 ± 2.3 (-9.5)	3.9 ± 2.1 (-9.2)	5.3 ± 1.4 (-6.8)
HF-3c-(0.5 s_8)	3.2 ± 2.3 (-7.4)	4.3 ± 2.2 (-7.4)	2.0 ± 2.1 (-7.2)	3.1 ± 1.7 (-4.6)
HF-3c-(0.27 s_8)	1.9 ± 2.3 (-5.0)	2.3 ± 2.1 (-5.0)	1.6 ± 2.2 (-4.9)	1.7 ± 2.0 (2.3)
HF-3c-(1.23 gCP)	5.6 ± 3.0 (-10.8)	7.3 ± 2.8 (-10.8)	3.4 ± 2.5 (-8.9)	6.3 ± 1.4 (-8.1)
B3LYP-D*/TZP	3.0 ± 1.9 (-6.0)	3.4 ± 1.9 (-6.0)	2.3 ± 1.8 (-5.8)	3.4 ± 2.2 (-4.8)

Table 2. Statistical summary for cohesive energies of the molecular crystals in the X23 set. MAE, SD and MAX of the ΔE_c evaluated at the HF-3c, B3LYP-D*/TZP, LMP2/p-aug-6-31G(d,p) and SP-B3LYP-D* levels of theory. For the HF-3c case, the results obtained by different scaling of the dispersion and gCP terms are also reported. For comparison, we have also included the statistical analysis for the ΔE_c at the PBE0-MBD/CBS, PBE-D3/CBS, PBE-D3-gCP/SVP and B3LYP-D3-gCP/SVP levels of theory.[33,67] The statistics is reported for both absolute errors (in kJ·mol^{-1}) and relative absolute percentage errors by using the following format MAE ± SD (MAX).

Method	All (X23)	Dispersive	H-bond	Mixed
Statistics in kJ·mol^{-1}				
HF-3c	8.2 ± 8.8 (21.3)	10.3 ± 7.9 (18.7)	7.0 ± 9.9 (21.3)	5.5 ± 6.6 (12.0)
S-HF-3c	6.9 ± 8.0 (13.9)	4.5 ± 6.0 (-13.2)	9.3 ± 9.8 (13.9)	7.8 ± 8.5 (-13.6)
HF-3c-(0.5 s_8)	8.8 ± 8.1 (-20.0)	6.2 ± 5.9 (-18.4)	10.7 ± 9.9 (-20.0)	11.0 ± 9.8 (-19.8)
HF-3c-(0.27 s_8)	13.1 ± 8.7 (-26.6)	12.1 ± 6.6 (-24.0)	13 ± 10 (-27)	16 ± 11 (-26)
HF-3c-(1.23 gCP)	8.4 ± 9.6 (-18.2)	8.1 ± 8.4 (13.0)	9.1 ± 8.9 (-18.2)	7.5 ± 9.5 (-13.5)
B3LYP-D*/TZP	4.6 ± 6.0 (-17.9)	6.2 ± 7.4 (-17.9)	3.6 ± 4.1 (6.1)	2.7 ± 2.4 (-5.4)
LMP2/aug-6-31G(d,p)	9 ± 11 (26)	10 ± 13 (26.3)	9.5 ± 7.1 (-23.7)	4.2 ± 4.9 (11.5)
SP-B3LYP-D*	5.2 ± 5.8 (-15.6)	6.4 ± 7.0 (-15.6)	4.3 ± 5.2 (-10.4)	4.3 ± 3.0 (-7.7)
PBE0-MBD/CBS	4.0 ± 4.7 (9.2)	4.9 ± 5.8 (9.2)	3.4 ± 3.5 (9.1)	3.1 ± 2.2 (4.7)
PBE-D3/CBS[a]	3.9 ± 4.9 (13.8)	2.7 ± 3.6 (-7.5)	5.2 ± 4.9 (13.8)	4.0 ± 3.8 (5.0)
PBE-D3-gCP/SVP[a]	10 ± 12 (-32)	7.8 ± 8.2 (-16.3)	14 ± 18 (-32)	6.0 ± 7.1 (7.5)
B3LYP-D3-gCP/SVP[a]	7.8 ± 9.0 (16.7)	8.7 ± 9.6 (16.7)	8 ± 10 (-16)	5.2 ± 3.0 (8.8)
Statistics in percentage				
HF-3c	11 ± 11 (22)	14.7 ± 9.5 (21.2)	9 ± 11 (22)	5.9 ± 7.2 (13.8)
S-HF-3c	7.9 ± 8.8 (-14.9)	6.3 ± 7.8 (-14.9)	10 ± 11 (14)	6.2 ± 6.9 (-10.0)
HF-3c-(0.5 s_8)	9.6 ± 8.1 (-20.8)	8.2 ± 7.0 (-20.8)	12 ± 10 (-17)	8.5 ± 6.7 (-14.6)
HF-3c-(0.27 s_8)	15.0 ± 7.9 (-27.1)	16.5 ± 6.3 (-27.1)	14 ± 10 (-22)	13.1 ± 6.6 (-19.5)
HF-3c-(1.23 gCP)	10 ± 11 (16)	11 ± 11 (16)	10.2 ± 9.5 (-14.4)	6.2 ± 8.3 (-9.9)
B3LYP-D*/TZP	5.7 ± 7.2 (-16.4)	8.6 ± 8.7 (-16.4)	4.1 ± 4.3 (6.0)	2.3 ± 2.0 (-4.3)
LMP2/p-aug-6-	11 ± 14 (43)	15 ± 19 (43)	10.4 ± 5.8 (-18.2)	3.2 ± 2.7 (7.1)

31G(d,p)

SP- B3LYP-D*	6.4 ± 7.0 (-15.9)	8.9 ± 8.4 (-15.9)	4.9 ± 5.4 (-8.0)	3.4 ± 1.8 (-4.8)
PBE0-MBD	5.7 ± 8.2 (-25.4)	8 ± 11 (-25)	4.2 ± 4.3 (11.4)	2.7 ± 2.3 (5.3)
PBE-D3/CBS[a]	5.1 ± 6.7 (17.3)	4.1 ± 5.3 (11.3)	6.8 ± 6.7 (17.3)	3.9 ± 3.4 (5.8)
PBE-D3-gCP/SVP[a]	14 ± 20 (60)	14 ± 20 (60)	17 ± 24 (46)	5.7 ± 6.7 (8.7)
B3LYP-D3-gCP/SVP[a]	11 ± 15 (43)	14 ± 19 (43)	10 ± 14 (33)	5.4 ± 4.0 (10.1)

[a] ΔE_c evaluated by keeping the unit cell parameters fixed to the experimental values.

Table 3. Statistical summary for sublimation enthalpies of the molecular crystals in the X23 set. MAE, SD and MAX of ΔH evaluated at the HF-3c and S-HF-3c levels of theory. ΔH* results refer to results obtained with scaled frequencies (see text for details). The statistics is reported for both absolute errors (in kJ·mol^{-1}) and relative absolute percentage errors by using the following format MAE ± SD (MAX).

	HF-3c	S-HF-3c
Statistics in kJ·mol^{-1}		
ΔH	8.6 ± 9.4 (21.1)	7.3 ± 8.3 (-14.4)
ΔH*	8.4 ± 9.3 (20.7)	7.3 ± 8.2 (-14.5)
Statistics in percentage		
ΔH	13 ± 13 (30)	9 ± 10 (-17)
ΔH*	12 ± 13 (29)	9 ± 10 (-17)

Table 4. Statistical summary for unit cell volumes of the molecular crystals in the G60 set. MAE, SD and MAX of the optimized cell volumes evaluated at the HF-3c, S-HF-3c and HF-3c-(0.27 s_8) levels of theory. The statistics is reported for both absolute errors (in $Å^3$) and relative absolute percentage errors by using the following format MAE ± SD (MAX).

Method	All (G60)	Dispersive	H-bond	Mixed
Statistics in $Å^3$				
HF-3c	45 ± 36 (-156)	49 ± 38 (-156)	9.3 ± 4.0 (-15.5)	47 ± 28 (-98)
S-HF-3c	30 ± 32 (-115)	33 ± 35 (-115)	3.8 ± 3.4 (-8.0)	30 ± 23 (-75)
HF-3c-(0.27 s_8)	24 ± 36 (134)	30 ± 42 (134)	6.4 ± 6.1 (16.6)	13 ± 19 (-41)
Statistics in percentage				
HF-3c	6.9 ± 4.2 (-17.2)	7.1 ± 4.6 (-17.2)	4.6 ± 1.2 (-6.1)	7.2 ± 3.2 (-11.8)
S-HF-3c	4.7 ± 4.2 (-14.2)	5.1 ± 4.7 (-14.2)	1.9 ± 1.5 (-3.2)	4.7 ± 3.0 (-9.1)
HF-3c-(0.27 s_8)	3.5 ± 4.5 (11.5)	4.0 ± 4.9 (11.5)	3.2 ± 3.2 (8.6)	2.0 ± 2.7 (-4.9)

Table 5. Statistical summary for cohesive energies of the molecular crystals in the G60 set. MAE, SD and MAX of the ΔE_c as evaluated at the HF-3c, S-HF-3c and SP-B3LYP-D* levels of theory. The statistical analysis for the ΔE_c at the B3LYP-D*/6-31G(d,p) level is also reported. The statistics is reported for both absolute errors (in kJ·mol^{-1}) and relative absolute percentage errors by using the following format MAE ± SD (MAX).

Method	All (G60)	Dispersive	H-bond	Mixed
Statistics in kJ·mol^{-1}				
HF-3c	12 ± 15 (-41)	13 ± 16 (-41)	5.4 ± 8.3 (16.9)	13 ± 15 (34)
S-HF-3c	12 ± 14 (-57)	13 ± 15 (-57)	8.8 ± 7.6 (10.8)	11 ± 14 (-34)
SP-B3LYP-D*	8.8 ± 7.6 (-25.7)	9.6 ± 7.4 (-25.7)	4.4 ± 4.3 (-6.6)	8.3 ± 8.5 (-21.0)
B3LYP-D*/6-31G*[a]	10 ± 12 (-37)	10.4 ± 9.0 (-36.7)	13 ± 11 (32)	9 ± 12 (26)
Statistics in percentage				
HF-3c	12 ± 14 (36)	13 ± 15 (36)	6.0 ± 8.9 (17.6)	11 ± 12 (27)
S-HF-3c	11 ± 12 (-33)	11 ± 12 (-33)	10.0 ± 8.4 (-12.9)	9 ± 11 (-26)
SP-B3LYP-D*	8.6 ± 7.1 (-25.7)	9.6 ± 7.4 (-25.7)	5.2 ± 5.2 (-9.9)	6.6 ± 6.7 (-16.1)
B3LYP-D*/6-31G*[a]	10 ± 11 (34)	10.3 ± 8.2 (-32.2)	13 ± 11 (34)	7.1 ± 9.5 (20.5)

[a] BSSE corrected ΔE_c calculated by keeping the crystal and molecules geometries fixed to the experiments, from ref. [70]

Table 6. Comparison between HF-3c, S-HF-3c, HF-3c-(0.27 s_8) and B3LYP-D*/TZP for predicted intermolecular distances (in Å) of a few selected molecular crystals. CM is the center of mass of the benzene ring.

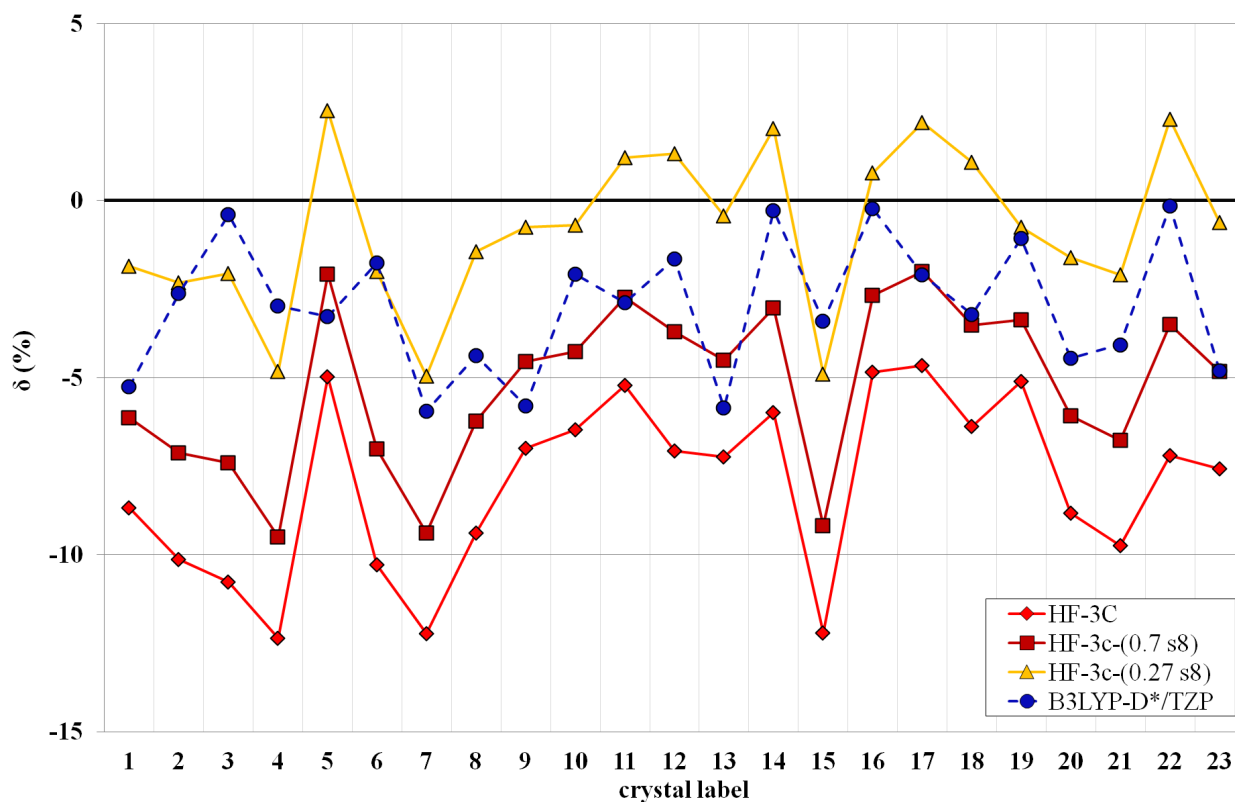|	HF-3c	S-HF-3c	HF-3c-(0.27 s8)	B3LYP-D*/TZP	EXP
Urea[74]					
O-H1(H4)	1.898	1.921	1.956	1.985	1.992
O-H2(H3)	2.014	2.025	2.043	2.053	2.058
Formamide[75]					
O1-H1 (O2-H2)	1.828	1.841	1.863	1.917	1.910
O3-H3	1.851	1.862	1.875	1.872	1.820
O1-H5 (O4-H4)	2.397	2.453	2.561	2.530	2.439
Formic acid[72]					
O1-H1 (O3-H3)	1.626	1.634	1.643	1.604	1.613
O2-H2	2.269	2.269	2.270	2.552	2.549
Benzene[73]					
CM-H1	2.542	2.607	2.706	2.695	2.702
CM-H2	3.416	3.468	3.556	3.595	3.575

Figure 1. Relative deviation in percentage, $\delta_i(\%) = 100 \cdot \frac{|x_i| - |x_i^{exp}|}{|x_i^{exp}|}$, of the computed cell volumes from the experimental reference values for the X23 set as obtained at the HF-3c and the B3LYP-D*/TZP level of theory as well as for the scaled HF-3c-(0.7 s_8) [S-HF-3c] and HF-3c-(0.27 s_8) methods. See Table S5 of SI for details on labeling of the molecular crystals in the X23 set.
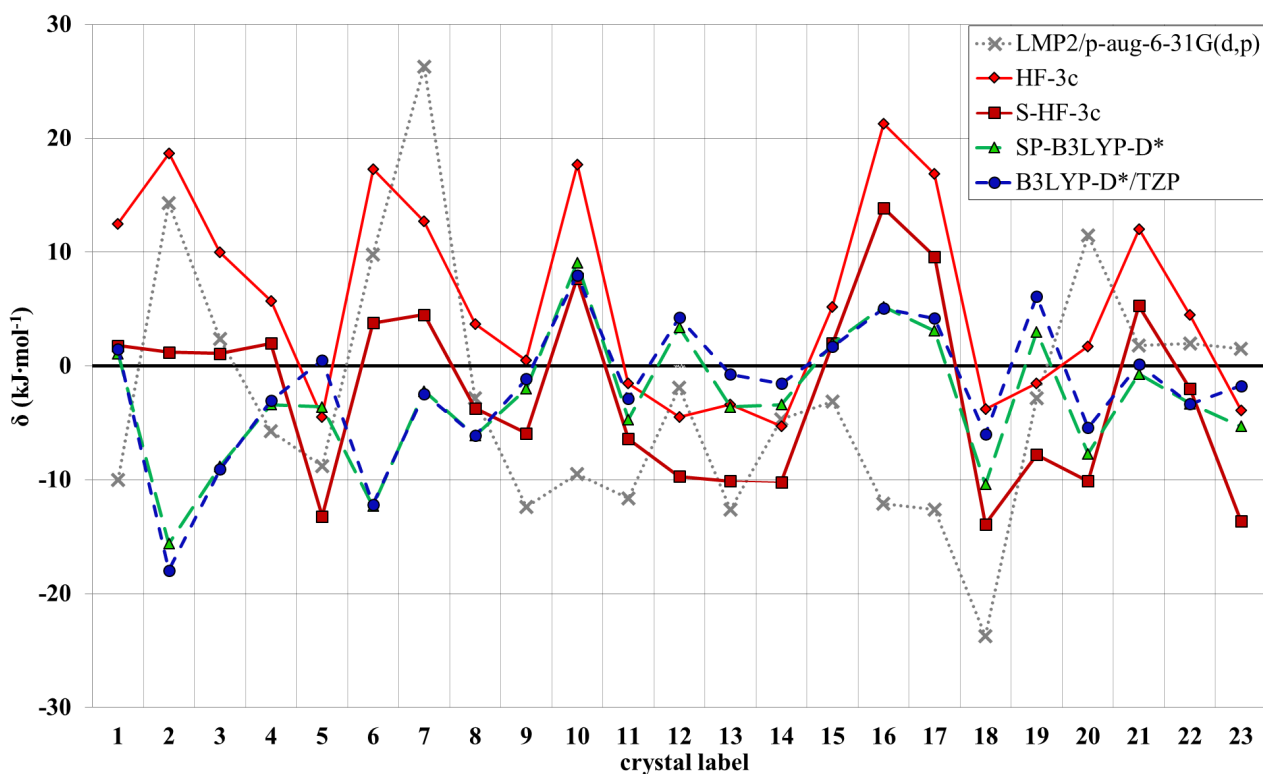
Figure 2. Deviation ($\delta_i = |x_i| - |x_i^{exp}|$) of the ΔE_c from the thermodynamically corrected experimental cohesive energies for the X23 set as computed at the LMP2/p-aug-6-31G(d,p), HF-3c, S-HF-3c, SP-B3LYP-D* and B3LYP-D*/TZP levels of theory. See Table S5 of SI for details on labeling of the molecular crystals in the X23 set.
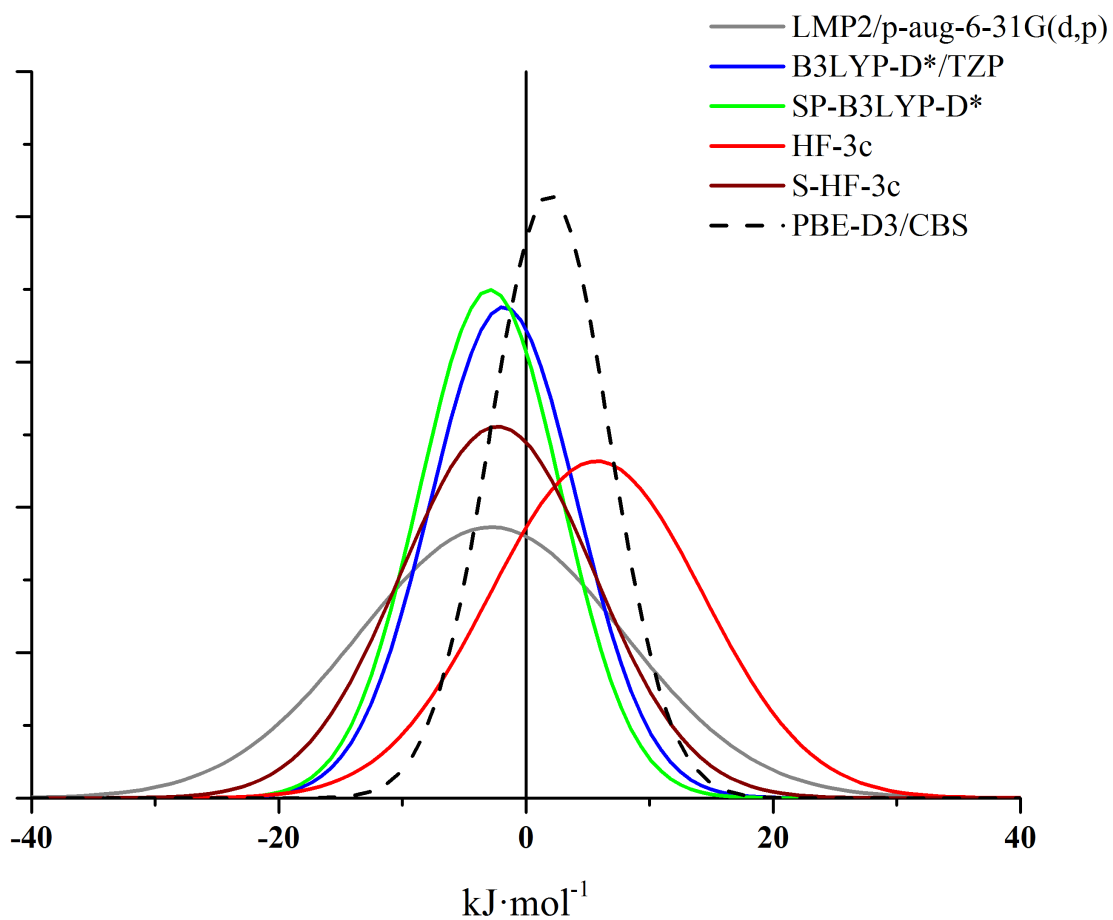
Figure 3. Normal error distribution of the deviation of theoretically predicted cohesive energies from experimental data for the X23 set (see Table 1). Negative values mean underbinding while positive values indicate overbinding. PBE-D3/CBS data from ref. [67].
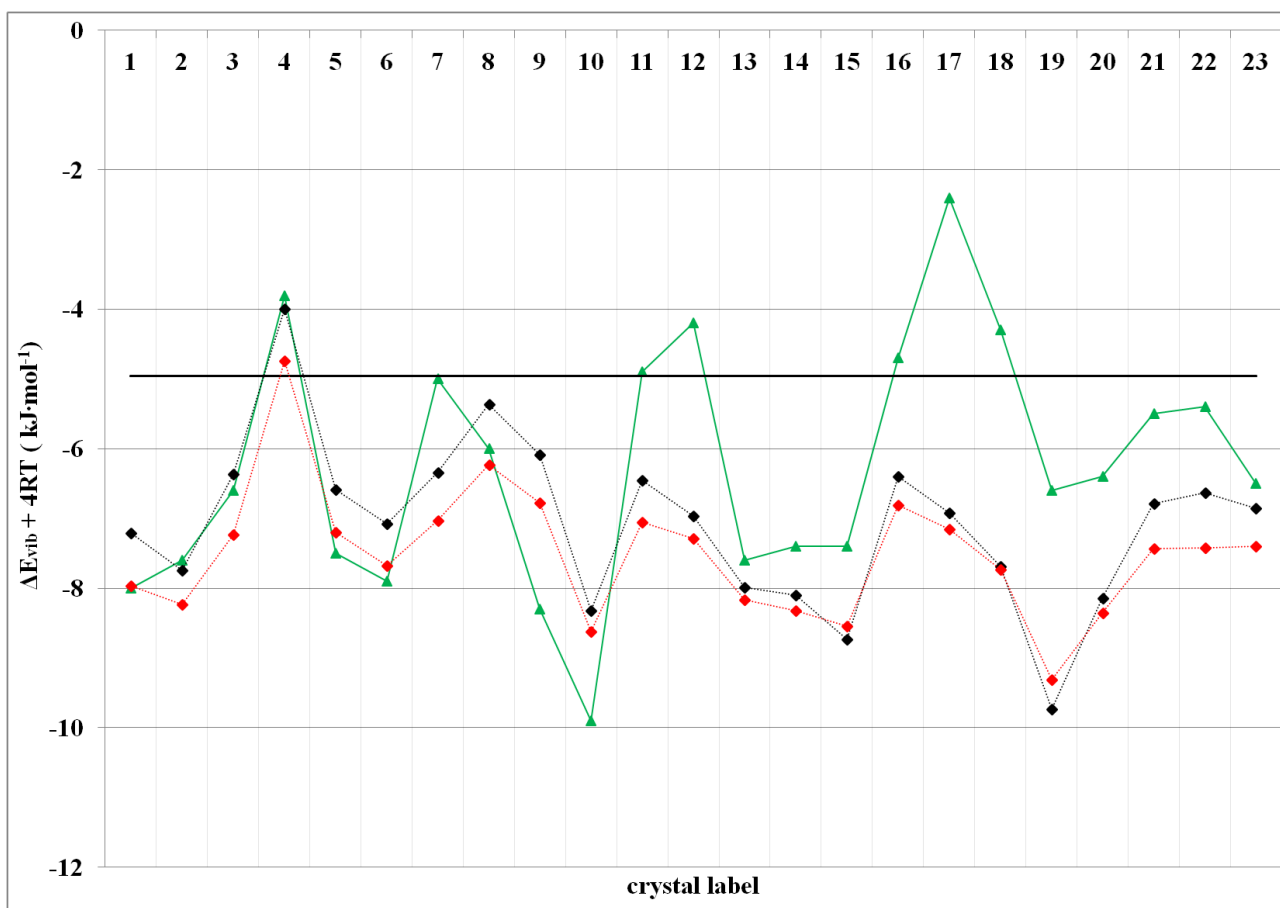
Figure 4. Comparison of the thermal correction to enthalpy ($\Delta E_{vib} + 4RT$) for the X23 set as evaluated at S-HF-3c (red squares, dotted red line) and PBE+TS level of theory (green triangle, solid green line) through the Einstein and supercell method, respectively.[33] The usually adopted 2RT value is also shown as black solid line. In addition, the results for the S-HF-3c level of theory with scaled vibrational frequencies are also reported (black squares, black dotted line). The temperature is set at 298.15 K. For details of crystal labeling see Table S5 of SI.
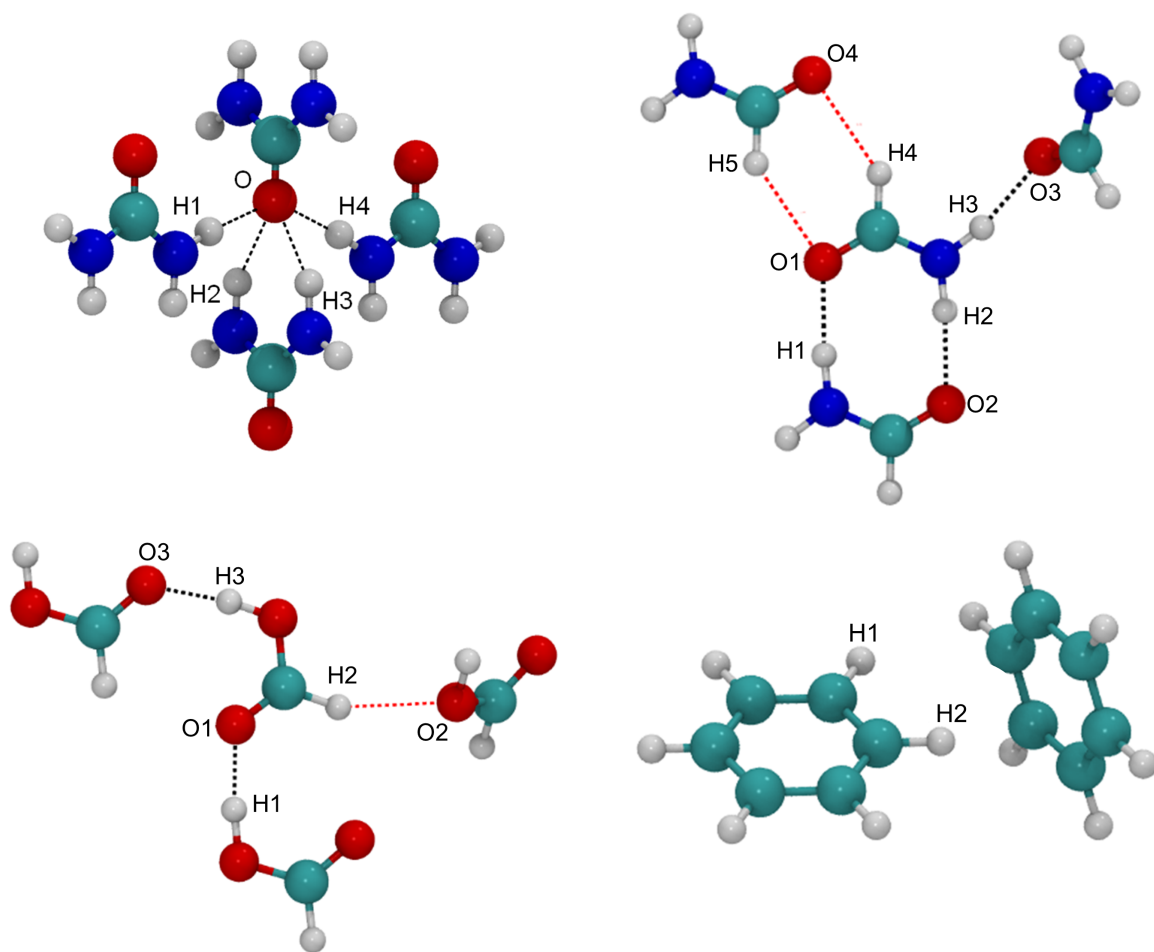
Figure 5. Details of the geometries of the urea, formamide, formic acid and benzene molecular crystals. Carbon is colored in turquoise, hydrogen in light gray, oxygen in red and nitrogen is blue.

Bibliography

(1)   London, F. The General Theory of Molecular Forces. *Trans. Faraday Soc* **1937**, *33*, 8b – 26.

(2)   Stone, A. J. The Theory of Intermolecular Forces; Oxford University Press: Oxford, 2013; pp 1–352.

(3)   Kaplan, I. G. Intermolecular Interactions: Physical Picture, Computational Methods and Model Potentials; John Wiley & Sons, Ltd.: Chichester, 2006; pp 1–367.

(4)   Neumann, M. A.; Leusen, F. J. J.; Kendrick, J. A Major Advance in Crystal Structure Prediction. *Angew. Chemie - Int. Ed.* **2008**, *47*, 2427–2430.

(5)   Reilly, A. M. *et al.* Report on the Sixth Blind Test of Organic Crystal-Structure Prediction Methods. *Acta Cryst. B* **2016**, accepted.

(6)   Price, S. L. Predicting Crystal Structures of Organic Compounds. *Chem. Soc. Rev.* **2014**, *43*, 2098–2111.

(7)   Beran, G. J. O.; Wen, S.; Nanda, K.; Huang, Y.; Heit, Y. Accurate and Robust Molecular Crystal Modeling Using Fragment-Based Electronic Structure Methods. *Top Curr Chem* **2014**, *345*, 59–93.

(8)   Block, S.; Weir, C. E.; Piermarini, G. J. Polymorphism in Benzene, Naphthalene, and Anthracene at High Pressure. *Science* **1970**, *169*, 586.

(9)   Grimme, S. Density Functional Theory with London Dispersion Corrections. *Wiley Interdiscip. Rev. Comput. Mol. Sci.* **2011**, *1*, 211–228.

(10)   Burns, L. A.; Vázquez-Mayagoitia, Á.; Sumpter, B. G.; Sherrill, C. D. Density-Functional Approaches to Noncovalent Interactions: A Comparison of Dispersion Corrections (DFT-D), Exchange-Hole Dipole Moment (XDM) Theory, and Specialized Functionals. *J. Chem. Phys.* **2011**, *134*, 084107.

(11)   Klimeš, J.; Michaelides, A. Perspective: Advances and Challenges in Treating van Der Waals Dispersion Forces in Density Functional Theory. *J. Chem. Phys.* **2012**, *137*, 120901.

(12)   Grimme, S.; Hansen, A.; Brandenburg, J. G.; Bannwarth, C. Dispersion-Corrected Mean-Field Electronic Structure Methods. *Chem. Rev.* **2016**, *116*, 5105–5154.

(13)   Woods, L. M.; Dalvit, D. A. R.; Tkatchenko, A.; Rodriguez-Lopez, P.; Rodriguez, A. W.; Podgornik, R. *Rev. Mod. Phys* **2016**, accepted.

(14)   Grimme, S. Semiempirical GGA-Type Density Functional Constructed with a Long-Range Dispersion Correction. *J. Comput. Chem.* **2006**, *27*, 1787–1799.

(15)   Moellmann, J.; Grimme, S. DFT-D3 Study of Some Molecular Crystals. *J. Phys. Chem. C* **2014**, *118*, 7615–7621.

(16) Grimme, S.; Antony, J.; Ehrlich, S.; Krieg, H. A Consistent and Accurate Ab Initio Parametrization of Density Functional Dispersion Correction (DFT-D) for the 94 Elements H-Pu. *J. Chem. Phys.* **2010**, *132*, 154104.

(17) Becke, A. D.; Johnson, E. R. A Density-Functional Model of the Dispersion Interaction. *J. Chem. Phys.* **2005**, *123*, 154101.

(18) Tkatchenko, A.; DiStasio, R. A.; Car, R.; Scheffler, M. Accurate and Efficient Method for Many-Body van Der Waals Interactions. *Phys. Rev. Lett.* **2012**, *108*, 236402.

(19) Sure, R.; Grimme, S. Corrected Small Basis Set Hartree-Fock Method for Large Systems. *J. Comput. Chem.* **2013**, *34*, 1672–1685.

(20) Brandenburg, J. G.; Hochheim, M.; Bredow, T.; Grimme, S. Low-Cost Quantum Chemical Methods for Noncovalent Interactions. *J. Phys. Chem. Lett.* **2014**, *5*, 4275–4284.

(21) Brandenburg, J. G.; Grimme, S. Dispersion Corrected Hartree–Fock and Density Functional Theory for Organic Crystal Structure Prediction. *Top Curr Chem* **2014**, *345*, 1–24.

(22) Pisani, C.; Schütz, M.; Casassa, S.; Usvyat, D.; Maschio, L.; Lorenz, M.; Erba, A. Cryscor: A Program for the Post-Hartree–Fock Treatment of Periodic Systems. *Phys. Chem. Chem. Phys.* **2012**, *14*, 7615.

(23) Del Ben, M.; Hutter, J.; Vandevondele, J. Second-Order Møller-Plesset Perturbation Theory in the Condensed Phase: An Efficient and Massively Parallel Gaussian and Plane Waves Approach. *J. Chem. Theory Comput.* **2012**, *8*, 4177–4188.

(24) Marsman, M.; Grüneis, A.; Paier, J.; Kresse, G. Second-Order Møller-Plesset Perturbation Theory Applied to Extended Systems. I. Within the Projector-Augmented-Wave Formalism Using a Plane Wave Basis Set. *J. Chem. Phys.* **2009**, *130*, 184103.

(25) Booth, G. H.; Grüneis, A.; Kresse, G.; Alavi, A. Towards an Exact Description of Electronic Wavefunctions in Real Solids. *Nature* **2013**, *493*, 365.

(26) MacHer, M.; Klimeš, J.; Franchini, C.; Kresse, G. The Random Phase Approximation Applied to Ice. *J. Chem. Phys.* **2014**, *140*, 084502.

(27) Kresse, G.; Harl, J. Accurate Bulk Properties from Approximate Many-Body Techniques. *Phys. Rev. Lett.* **2009**, *103*, 056401.

(28) Sansone, G.; Civalleri, B.; Usvyat, D.; Toulouse, J.; Sharkas, K.; Maschio, L. Range-Separated Double-Hybrid Density-Functional Theory Applied to Periodic Systems. *J. Chem. Phys.* **2015**, *143*, 102811.

(29) Maschio, L.; Usvyat, D.; Schütz, M.; Civalleri, B. Periodic Local Møller-Plesset Second Order

Perturbation Theory Method Applied to Molecular Crystals: Study of Solid NH3 and CO2 Using Extended Basis Sets. *J. Chem. Phys.* **2010**, *132*, 134706.

(30)   Maschio, L.; Usvyat, D.; Civalleri, B. Ab Initio Study of van Der Waals and Hydrogen-Bonded Molecular Crystals with a Periodic Local-MP2 Method. *CrystEngComm* **2010**, *12*, 2429.

(31)   Sharkas, K.; Toulouse, J.; Maschio, L.; Civalleri, B. Double-Hybrid Density-Functional Theory Applied to Molecular Crystals. *J. Chem. Phys.* **2014**, *141*, 044105.

(32)   Otero-De-La-Roza, A.; Johnson, E. R. A Benchmark for Non-Covalent Interactions in Solids. *J. Chem. Phys.* **2012**, *137*, 054103.

(33)   Reilly, A. M.; Tkatchenko, A. Understanding the Role of Vibrations, Exact Exchange, and Many-Body van Der Waals Interactions in the Cohesive Properties of Molecular Crystals. *J. Chem. Phys.* **2013**, *139*, 024705.

(34)   Tatewaki, H.; Huzinaga, S. A Systematic Preparation of New Contracted Gaussian-Type Orbital Sets. III. Second-Row Atoms from Li through Ne. *J. Comput. Chem.* **1980**, *1*, 205–228.

(35)   Schäfer, A.; Horn, H.; Ahlrichs, R. Fully Optimized Contracted Gaussian Basis Sets for Atoms Li to Kr. *J. Chem. Phys.* **1992**, *97*, 2571.

(36)   Weigend, F.; Ahlrichs, R. Balanced Basis Sets of Split Valence, Triple Zeta Valence and Quadruple Zeta Valence Quality for H to Rn: Design and Assessment of Accuracy. *Phys. Chem. Chem. Phys.* **2005**, *7*, 3297–3305.

(37)   Johnson, E. R.; Becke, A. D. A Post-Hartree–Fock Model of Intermolecular Interactions. *J. Chem. Phys.* **2005**, *123*, 024101.

(38)   Kruse, H.; Grimme, S. A Geometrical Correction for the Inter- and Intra-Molecular Basis Set Superposition Error in Hartree-Fock and Density Functional Theory Calculations for Large Systems. *J. Chem. Phys.* **2012**, *136*, 154101.

(39)   Dovesi, R.; Orlando, R.; Erba, A.; Zicovich-Wilson, C. M.; Civalleri, B.; Casassa, S.; Maschio, L.; Ferrabone, M.; De La Pierre, M.; D'Arco, P.; Noël, Y.; Causà, M.; Rérat, M.; Kirtman, B. CRYSTAL14 : A Program for the Ab Initio Investigation of Crystalline Solids. *Int. J. Quantum Chem.* **2014**, *114*, 1287–1317.

(40)   Becke, A. D. Density-Functional Thermochemistry. III. The Role of Exact Exchange. *J. Chem. Phys.* **1993**, *98*, 5648–5652.

(41)   Lee, C.; Yang, W.; Parr, R. G. Development of the Colle-Salvetti Correlation-Energy Formula into a Functional of the Electron Density. *Phys. Rev. B* **1988**, *37*, 785–789.

(42)   Civalleri, B.; Zicovich-Wilson, C. M.; Valenzano, L.; Ugliengo, P. B3LYP Augmented with an

Empirical Dispersion Term (B3LYP-D*) as Applied to Molecular Crystals. *CrystEngComm* **2008**, *82*, 4–6.

(43) Muto, Y. The Force Between Nonpolar Molecules. *Proc. Phys. Math. Soc. Japan* **1944**, *17*, 629.

(44) Axilrod, B. M.; Teller, E. Interaction of the van Der Waals Type Between Three Atoms. *J. Chem. Phys.* **1943**, *11*, 299–300.

(45) Møller, C.; Plesset, M. S. Note on an Approximation Treatment for Many-Electron Systems. *Phys. Rev.* **1934**, *46*, 618–622.

(46) Usvyat, D.; Maschio, L.; Schütz, M. Periodic Local MP2 Method Employing Orbital Specific Virtuals. *J. Chem. Phys.* **2015**, *143*, 102805.

(47) Kurashige, Y.; Yang, J.; Chan, G. K.-L.; Manby, F. R. Optimization of Orbital-Specific Virtuals in Local Møller-Plesset Perturbation Theory. *J. Chem. Phys.* **2012**, *136*, 124106.

(48) Ugliengo, P.; Viterbo, D.; Chiari, G. MOLDRAW: Molecular Graphics on a Personal Computer. *Z. Krist.* **1993**, *207*, 9-23.

(49) Humphrey, W.; Dalke, A.; Schulten, K. VMD: Visual Molecular Dynamics. *J. Mol. Graph.* **1996**, *14*, 33–38.

(50) Broyden, C. G. The Convergence of a Class of Double-Rank Minimization Algorithms 1. General Considerations. *IMA J. Appl. Math.* **1970**, *6*, 76–90.

(51) Fletcher, R. A. New Approach to Variable Metric Algorithms. *Comput. J.* **1970**, *13*, 317–322.

(52) Shanno, D. F.; Kettler, P. C. Optimal Conditioning of Quasi-Newton Methods. *Math. Comput.* **1970**, *24*, 657–664.

(53) Dovesi, R.; Saunders, V. R.; Roetti, C.; Orlando, R.; Zicovich-Wilson, C. M.; Pascale, F.; Civalleri, B.; Doll, K.; Harrison, N. M.; Bush, I. J.; D'Arco, P.; Llunell, M.; Causà, M.; Noël, Y. *CRYSTAL14, User's Manual*; Università di Torino: Torino, Italy, 2014.

(54) Monkhorst, H. J.; Pack, J. D. Special Points for Brillouin-Zone Integration. *Phys. Rev. B.* **1976**, *8*, 5188–5192.

(55) Prencipe, M.; Pascale, F.; Zicovich-Wilson, C. M.; Saunders, V. R.; Orlando, R.; Dovesi, R. The Vibrational Spectra of Calcite (CaCO3): An Ab Inito Quantum-Mechanical Calculation. *Phys. Chem. Miner.* **2004**, *31*, 1–6.

(56) Boys, S. F.; Bernardi, F. The Calculation of Small Molecular Interactions by the Differences of Separate Total Energies. Some Procedures with Reduced Errors. *Mol. Phys.* **1970**, *19*, 553–566.

(57) Chickosa, J. S.; Acree, W. E. Enthalpies of Sublimation of Organic and Organometallic Compounds. 1910-2001. *J. Phys. Chem. Ref. Data* **2002**, *31*, 537–698.

(58) Chickos, J. S. Enthalpies of Sublimation after a Century of Measurement : A View as Seen through the Eyes of a Collector. *Netsu Sokutei* **2003**, *30*, 116–124.

(59) Grimme, S.; Brandenburg, J. G.; Bannwarth, C.; Hansen, A. Consistent Structures and Interactions by Density Functional Theory with Small Atomic Orbital Basis Sets. *J. Chem. Phys.* **2015**, *143*, 054107.

(60) Brandenburg, J. G.; Maas, T.; Grimme, S. Benchmarking DFT and Semiempirical Methods on Structures and Lattice Energies for Ten Ice Polymorphs. *J. Chem. Phys.* **2015**, *142*, 124104.

(61) Erba, A.; Maul, J.; Civalleri, B. Thermal Properties of Molecular Crystals through Dispersion-Corrected Quasi-Harmonic Ab Initio Calculations: The Case of Urea. *Chem. Commun.* **2016**, *52*, 1820–1823.

(62) Heit, Y. N.; Nanda, K. D.; Beran, G. J. O. Predicting Finite-Temperature Properties of Crystalline Carbon Dioxide from First Principles with Quantitative Accuracy. *Chem. Sci.* **2016**, *7*, 246–255.

(63) Bučko, T.; Lebègue, S.; Gould, T.; Ángyán, J. G. Many-Body Dispersion Corrections for Periodic Systems: An Efficient Reciprocal Space Implementation. *J. Phys. Condens. Matter* **2016**, *28*, 045201.

(64) Carter, D. J.; Rohl, A. L. Benchmarking Calculated Lattice Parameters and Energies of Molecular Crystals Using van Der Waals Density Functionals. *J. Chem. Theory Comput.* **2014**, *10*, 3423–3437.

(65) Sorescu, D. C.; Byrd, E. F. C.; Rice, B. M.; Jordan, K. D. Assessing the Performances of Dispersion-Corrected Density Functional Methods for Predicting the Crystallographic Properties of High Nitrogen Energetic Salts. *J. Chem. Theory Comput.* **2014**, *10*, 4982–4994.

(66) Brandenburg, J. G.; Grimme, S. Dispersion Corrected Hartree–Fock and Density Functional Theory for Organic Crystal Structure Prediction. In *Prediction and Calculation of Crystal Structures. Methods and Applications*; Atahan-Evrenk, Ş., Aspuru-Guzik, A., Eds.; Springer: Cambridge, 2013; pp 1–24.

(67) Brandenburg, J. G.; Alessio, M.; Civalleri, B.; Peintinger, M. F.; Bredow, T.; Grimme, S. Geometrical Correction for the Inter- and Intramolecular Basis Set Superposition Error in Periodic Density Functional Theory Calculations. *J. Phys. Chem. A* **2013**, *117*, 9282–9292.

(68) Riley, K. E.; Platts, J. a.; Řezáč, J.; Hobza, P.; Hill, J. G. Assessment of the Performance of MP2 and MP2 Variants for the Treatment of Noncovalent Interactions. *J. Phys. Chem. A* **2012**, *116*, 4159–4169.

(69) Cybulski, S. M.; Lytle, M. L. The Origin of Deficiency of the Supermolecule Second-Order Møller-Plesset Approach for Evaluating Interaction Energies. *J. Chem. Phys.* **2007**, *127*, 141102.

(70) Maschio, L.; Civalleri, B.; Ugliengo, P.; Gavezzotti, A. Intermolecular Interaction Energies in Molecular Crystals: Comparison and Agreement of Localized Møller-Plesset 2, Dispersion-Corrected Density Functional, and Classical Empirical Two-Body Calculations. *J. Phys. Chem. A* **2011**, *115*,

11179–11186.

(71)   Sinha, P.; Boesch, S. E.; Gu, C.; Wheeler, R. A.; Wilson, A. K. Harmonic Vibrational Frequencies: Scaling Factors for HF, B3LYP, and MP2 Methods in Combination with Correlation Consistent Basis Sets. *J. Phys. Chem. A* **2004**, *108*, 9213–9217.

(72)   Albinati, A.; Rouse, K. D.; Thomas, M. W. Neutron Powder Diffraction Analysis of Hydrogen-Bonded Solids. II. Structural Study of Formic Acid at 4.5 K. *Acta Crystallogr. Sect. B* **1978**, *34*, 2188.

(73)   Jeffrey, G. A.; Ruble, J. R.; McMullan, R. K.; Pople, J. A. The Crystal Structure of Deuterated Benzene. *Proc. R. Soc. Lond. A* **1987**, *414*, 47.

(74)   Swaminatha, S.; Craven, B. M.; McMullan, R. K. The Crystal Structure and Molecular Thermal Motion of Urea at 12, 60 and 123 K from Neutron Diffraction. *Acta Crystallogr. Sect. B Struct. Crystallogr. Cryst. Chem.* **1984**, *40*, 300.

(75)   Torrie, B. H.; O'Donovan, C.; Powell, B. M. Structure of Solid Formamide at 7 K. *Mol. Phys.* **1994**, *82*, 643.

(76)   Dobson, J. F. Beyond Pairwise Additivity in London Dispersion Interactions. *Int. J. Quantum Chem.* **2014**, *114*, 1157–1161.

(77)   Nyman, J.; Day, G. M. Static and Lattice Vibrational Energy Differences between Polymorphs. *CrystEngComm* **2015**, *17*, 5154–5165.

Table of Contents (TOC)

82 MOLECULAR CRYSTALS

LMP2
SP-B3LYP-D*
S-HF-3c
B3LYP-D*

G60 X23 K7

X23 COHESIVE ENERGY DEVIATION (kJ·mol^{-1})